Dispersion of the Sumatra Tsunami Waves in the Indian Ocean detected by satellite altimetry

by

Evgueni Kulikov

P.P. Shirshov Institute of Oceanology, Russian Academy of Sciences, Moscow[1]

At 00:59 UTC on December 26, 2004, a $M = 9.0$ megathrust earthquake occurred along 1000 km of the subduction zone west of Sumatra and Thailand in the Indian Ocean (Figure 1). The tsunami generated by this massive earthquake was responsible for over 200,000 deaths, millions of homeless people, and untold property and infrastructure damage along the exposed coasts of Indonesia, Thailand, Sri Lanka, India and the Maldives. Somalia, Kenya and other countries on the east coast of Africa were also significantly impacted by the waves. The tsunami waves propagated to the far corners of the global ocean and were recorded with amplitudes ranging from a few centimeters to several meters on the coasts of Australia, New Zealand, South Africa, the east and west coasts of North and South America, and the Pacific Islands (Alexander Rabinovich, pers. comm.).

Although previous attempts have had some success detecting relatively weak tsunamis in satellite altimeter data [cf. *Okal et al.*, 1999], the Sumatra event was the first major tsunami detected by satellite altimetry. Moreover, the event was observed by four satellite systems (TOPEX/POSEIDON, Jason, Envisat and Geosat) rather than just a single system. The Jason-satellite, operated jointly by NASA and the French space agency (CNES), was strategically placed during cycle 109, track 129 [*Gower*, 2005], providing accurate measurement of the tsunami wave height in the Indian Ocean. Here, we use sea surface altimetry data provided by the Jason-1 track to examine the dispersive characteristics of the open ocean tsunami waves as they propagated from the source area westward toward India and Sri Lanka.

The along-track sea level profile in Figure 2a is a filtered version of the original elevation record, formed by subtracting a background profile (Figure 2b) from the original along-track record. In this case, the background record is generated using a 150 km-long smoothing window applied to the previous cycle (#108). The probable tsunami source zone (the site of the initial wavefront) is shown by grey dashed elongated area in the figure. The satellite transversed this north to south track during the time period of 2: 51 to 3:02 UTC (from latitude 12° S to latitude 20°), or about

[1] Also at the Institute of Ocean Sciences, Sidney, BC, Canada

2 hours after the main earthquake shock. As indicated in Figure 1, the tsunami wave intersected the 2-hour wavefront as determined by the tsunami wave simulation provided by Kenji Satake of the National Institute of Advanced Industrial Science and Technology, Japan. Sea surface elevations shown in red and blue denote positive and negative wave displacement, respectively. The maximum wave crest of about 80 cm was associated with the second peak. The spatial scale of wave coverage was roughly 500-800 km. According to Rabinovich (pers. comm.), the first wave was maximum in all records near the source area, including the Maldives. The thick solid red line in Figure 2a shows the inverse 2-hour wavefront which has been calculated using as the starting point the location where the satellite track intersects the simulated wavefront. According to this calculation, the actual tsunami source would have been located to the north or north-east of this line.

Wavelet analysis of the observed wave elevations (Figure 2b) reveals that the high frequency components of the 2004 Indian Ocean tsunami were markedly dispersive. The leading edge of the wave components with 10-km wavelength were significantly delayed in comparison with the main wavefront components with about 1000 km wavelengths. It is also worth noting that oscillations for all frequencies (and wavenumbers) were abruptly dampened northward of 8° N (delineated by the vertical dashed line in the figure) The latter zone consists of short tsunami waves with wavelengths $L = T\sqrt{gH} \approx$ 1400 km, where $T = 2$ hours is the time of wave propagation, g is gravity, and $H \approx 4000$ m is the ocean depth. Based on this calculation, it is possible to state that the "boundary of the high-frequency wave generation zone" was located at between 7-8° N, in the region of the red line in Figure 1.

Figure 3 shows the tsunami signal two hours after the main shock, as determined from the difference between the altimetry profile of Cycle 109 and a smoothed version of the altimetry profile of the previous track (Cycle 108). The spatial extent of the wave field is remarkable. Besides the twin-peak first maximum, there is a gradual maximum about 800 km northward from the first. There is also an additional sharp maximum located between these main maxima. The leading edge of the extracted tsunami signal (the first forked maximum) is probably associated with the initial tsunami signal in the source area. Such a complicated structure for the tsunami "signature" is probably related to a complex rupture process that had a start-stop character [*Borges et al.*, 2005]: The rupture developed during a period of more than 200 sec as an interruptive-continuous process spreading northward. The fact that the formation of the co-seismic sea floor displacement had such a long formation time means that it cannot be treated as "instantaneous" in the normal sense of tsunami dynamics. In other words, the piston-like

mechanism that is normally used in tsunami numerical modeling is not quite valid for the complicated Sumatra wave source.

The time step in Figure 3 gives the time scale for estimating the main periods of the tsunami waves recorded at a fixed location in the open ocean, for example at an island tide gauge. According to this figure, most of the energy was associated with a wave period of about 50-60 min. Although the satellite trace does not coincide with the wave ray trace, we assume that this period (50-60 min) is the fundamental period for the Sumatra tsunami waves. This assumption is in good agreement with spectral analyses of the tide gauge tsunami records (Alexander Rabinovich, pers. comm.). The bottom panel presents results from frequency band-pass analysis of the tsunami signal and clearly indicates the spatial shift (time delay) of the short wave components compared to the leading wavefront.

The effect of tsunami wave dispersion in the open ocean has been previously reported by *González and Kulikov* [1993] and *Kulikov and González* [1995]. Small tsunami waves (of about 2 cm amplitude) arising from the earthquake March 6, 1988 in the Alaska Bight have been recorded by precise bottom pressure gauges located in about 1000 km from the source area. The seismic source was of small horizontal extent and, accordingly, generated relatively short, highly dispersive tsunami waves. The amplitude and frequency modulation of the observed tsunami bottom pressure records has been shown to be due to the dispersion predicted by the linear wave theory.

González and Kulikov [1993] compared the observed dispersion with a theoretical estimate of the wave dispersion derived from the group velocity of the waves. From the generalized dispersion relation for water waves [*LeBlond and Mysak*, 1978],

$$\omega^2 = gk \tanh(kH), \tag{1}$$

where ω is the angular frequency, k is the wavenumber, and H is the local water depth. The phase speed for these waves is

$$c = \omega / k = \sqrt{\frac{g}{k} \tanh(kH)}, \tag{2}$$

and the group speed (which characterizes the wave dispersion) is

$$c_g = \frac{\partial \omega}{\partial k} = \frac{\omega}{2k}\left(1 + \frac{2kH}{\sinh(2kH)}\right). \qquad (3)$$

Wavelet analysis used in [*Kulikov and González*, 1995] clearly revealed this effect of delaying high frequency wave components with the time-delay $t = L / c_g(\omega)$, where L is a wave travel distance and group velocity $c_g(\omega)$ is given by (3). A simple wave model developed for comparison with the data was consistent with the sea floor displacement estimated from a seismic fault plane deformation model (western-subsidence-uplift dipole).

Okal et al. [1999], who appear to have been the first to detect fluctuations in the sea surface due to a tsunami wave field (associated with the 1992 Nicaragua tsunami), also found evidence of tsunami wave dispersion; specifically 9% dispersion for wave periods of 850 and 350 s, which is close to the value of 7.7% measured by *González and Kulikov* [1993]. The high resolution altimeter data from Jason-1 enables us to examine this effect more precisely for a much stronger and much larger-scale earthquake and associated tsunami events.

A similar analysis for "spatial dispersion" has been undertaken in the wavenumber domain for the tsunami profile derived from the Jason-1 altimetry. The track line crosses the calculated wavefront at an angle of about 30°-40° to the tsunami rays. Numerical modeling of the Sumatra wave event by Titov (2005), which is based on an extensive source area (about 1100 km in length), presents several patterns of the wavefront (these model results are available now in graphic form on the NOAA website http://www.pmel.noaa.gov/tsunami/indo_1204.html). The orientation of the satellite track relative to the tsunami wavefronts is assumed to be close to normal (taken as the direction to the middle of aftershock area). The dispersion curve in Figure 2 indicates the wavefronts for different spectral components. To the right (north) of the wave-affected area of the figure is located an empty wave zone separated from the other area by a vertical dashed line. This feature may have arisen as a result of the strong directivity of this specific tsunami source. There were no highly frequency waves propagating in the northward direction, a feature which is probably related to the high directional character of the source. Most of the energy was apparently directed in a southwestward direction, in good agreement with the numerical simulations of Titov, PMEL [http://www.pmel.noaa.gov/tsunami/indo_1204.html)]

Conclusions

The tsunami generated by the 26 December 2004 Indian Ocean earthquake had a horizontal extent of about 1400 km. Such a large spatial dimension is apparently related to an unusually extensive crustal rupture. This supposition is in agreement with the result of preliminary study by *Borges et al.* [2005]) showing that the duration of the Sumatra earthquake rupture process exceeded 200 s. This, in turn, means that the rupture extension was about 1000 km.

This analysis demonstrates that the tsunami waves propagating southwestward across the Indian Ocean two hours after the main shock were noticeably dispersive. Together with earlier results [*González and Kulikov*, 1993; *Kulikov and González*, 1995; *Okal et al.*, 1999] this, in turn, brings into question the accuracy of the model used for numerical simulations of tsunamis. Normally these models are based on the shallow water approximation which ignores the effect of linear wave dispersion. However, according to the results reported here, such dispersion could be significant for amplitude estimation in transoceanic tsunami propagation.

Acknowledgments

I would like to thank Richard Thomson and Alexander Rabinovich for their comments and editing of the text,

References

Borges J.F., B. Caldeira, and M. Bezzeghoud, Source rupture process of the Great Sumatra, Indonesia Earthquake (M_w = 8.9) of 26 December 2004. Preliminary Results, Universidade de Évora, Portugal, http://www.cge.uevora.pt/, 2005.

González, F.I., and Ye.A. Kulikov, Tsunami dispersion observed in the deep ocean, in *Tsunamis in the World*, edited by S. Tinti, pp.7-16, Kluwer Acad., Dordrecht, 1993.

Gower, J., Jason 1 detects the Dec 26 2004 tsunami, *EOS*, *86* (3), 2005.

Kulikov, Ye.A., and F.I. González, Recovery of the shape of a tsunami signal at the source from measurements of oscillations in the ocean level by a remote hydrostatic pressure sensor. *Trans. (Doklady) Russian Acad. Sci., Earth Sci. Sect*., *345A*, 585-591, 1996.

LeBlond, P.H., and L.A. Mysak, *Waves in the Ocean*, Elsevier Oceanography Series, Amsterdam, 602 p., 1978.

Okal, E.A., A. Piatanesi, and P. Heinrich, Tsunami detection by satellite altimetry, *J. Geophys. Res.-Solid Earth*, *104* (1), 599-615, 1999.

Captions to Figures

Figure 1. Calculated tsunami wavefront in the Indian Ocean about two hours after the Sumatra Earthquake of December 26, 2004 (courtesy of Kenji Satake, NIAIS, Japan) together with the altimetry sea-level profile taken along Track 129 of the Jason-1 satellite during Cycle 109. Positions of the main shock and following aftershocks are indicated. The solid red line shows inverse 2-hour wavefront, calculated from the leading edge of the wavefront point on the satellite track. Grey region denotes the probable tsunami source area.

Figure 2. (a) Altimetry sea-level taken along track 129 of the Jason-1 satellite for Cycle 109 and along the same track 10 days earlier for Cycle 108; and (b) wavelet analysis of the sea level profile in (a). The solid line is the theoretical dispersion curve derived using equation (3). The vertical dashed line marks the boundary of the "wave affected" area associated with a seismotectonic source having spatial coverage scale $L \approx T\sqrt{gH}$ (for $T = 2$ hours). To the north of this boundary is a "wave void region" into which no waves have propagated. Letter "*T*" indicates the tsunami wavefront.

Figure 3. The altimetry sea-level profile and set of band-pass filtered signals derived from the original record. The central band-pass filter wave numbers are shown. Arrows denote the region of sea level disturbance created by the seismic source. The travel-time and horizontal scales are presented in the upper panel.

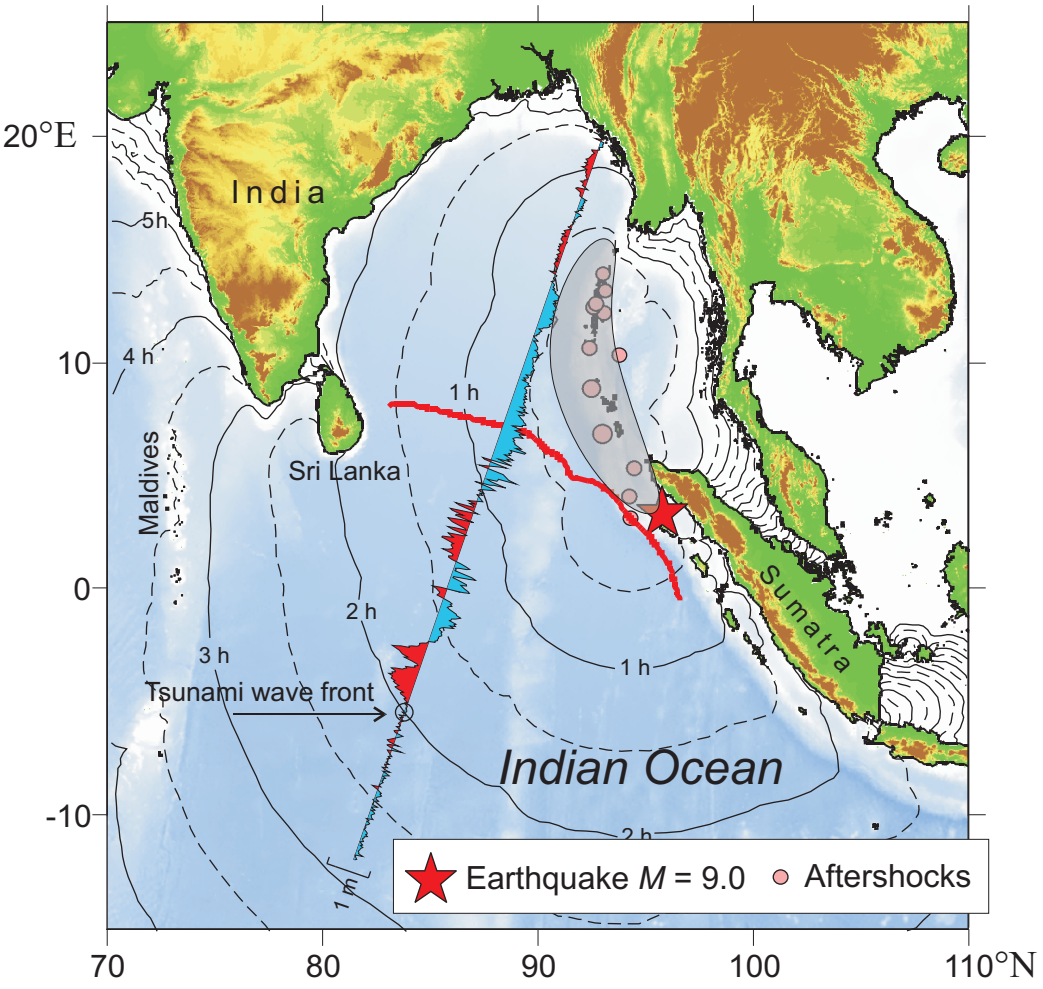
20°E
10
0
-10
70
80
90
100
110°N
India
5h
4 h
1 h
Maldives
Sri Lanka
2 h
3 h
Tsunami wave front
1 h
Sumatra
Indian Ocean
2 h
1 h
Earthquake M = 9.0
Aftershocks

Figure 1

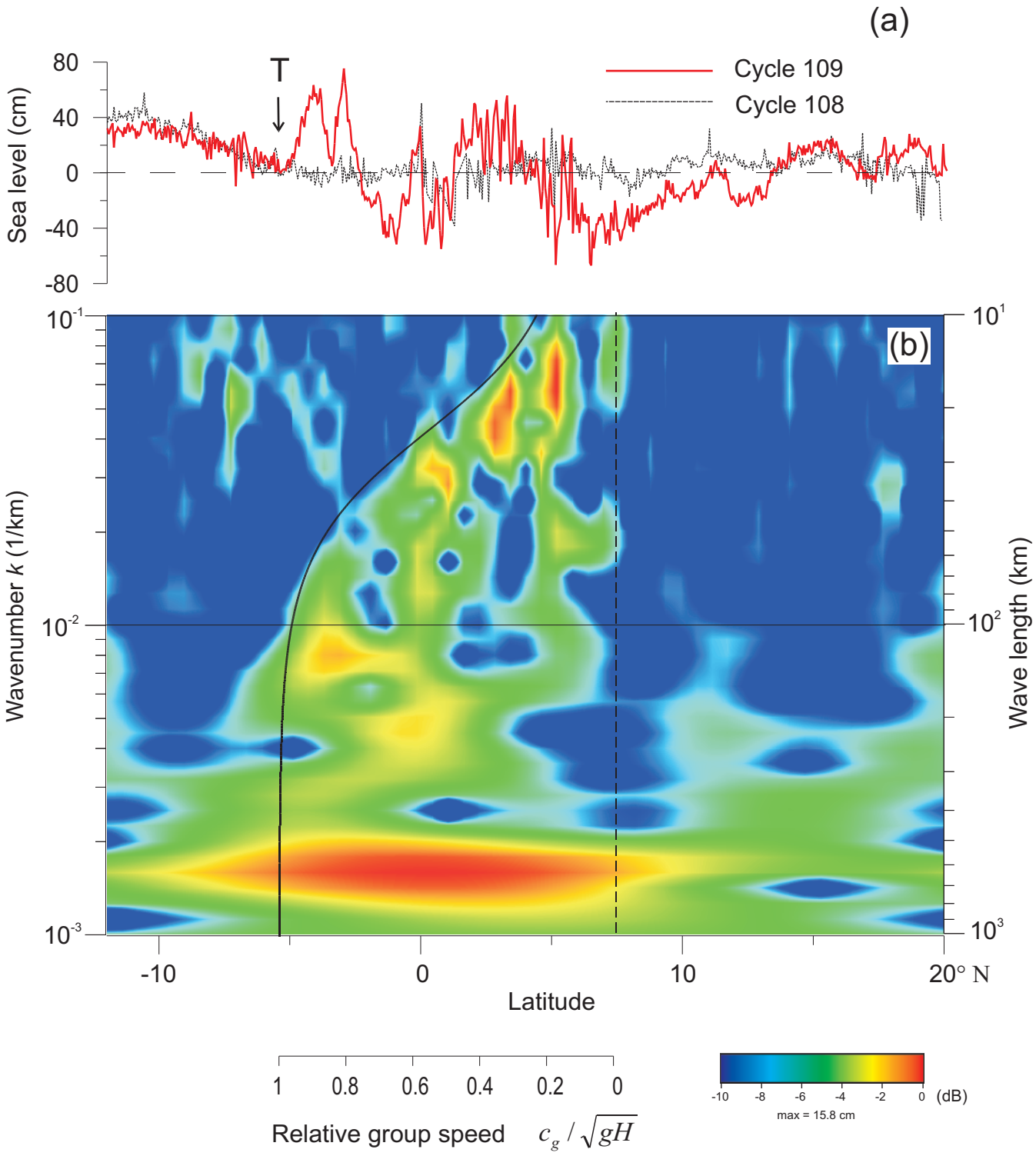
(a)
Sea level (cm)
80
40
0
-40
-80
T
Cycle 109
Cycle 108
(b)
Wavenumber k (1/km)
10-1
10-2
10-3
Wave length (km)
101
102
103
-10
0
10
20° N
Latitude
1
0.8
0.6
0.4
0.2
0
Relative group speed $c_g / \sqrt{gH}$
-10
-8
-6
-4
-2
0
(dB)
max = 15.8 cm

Figure 2

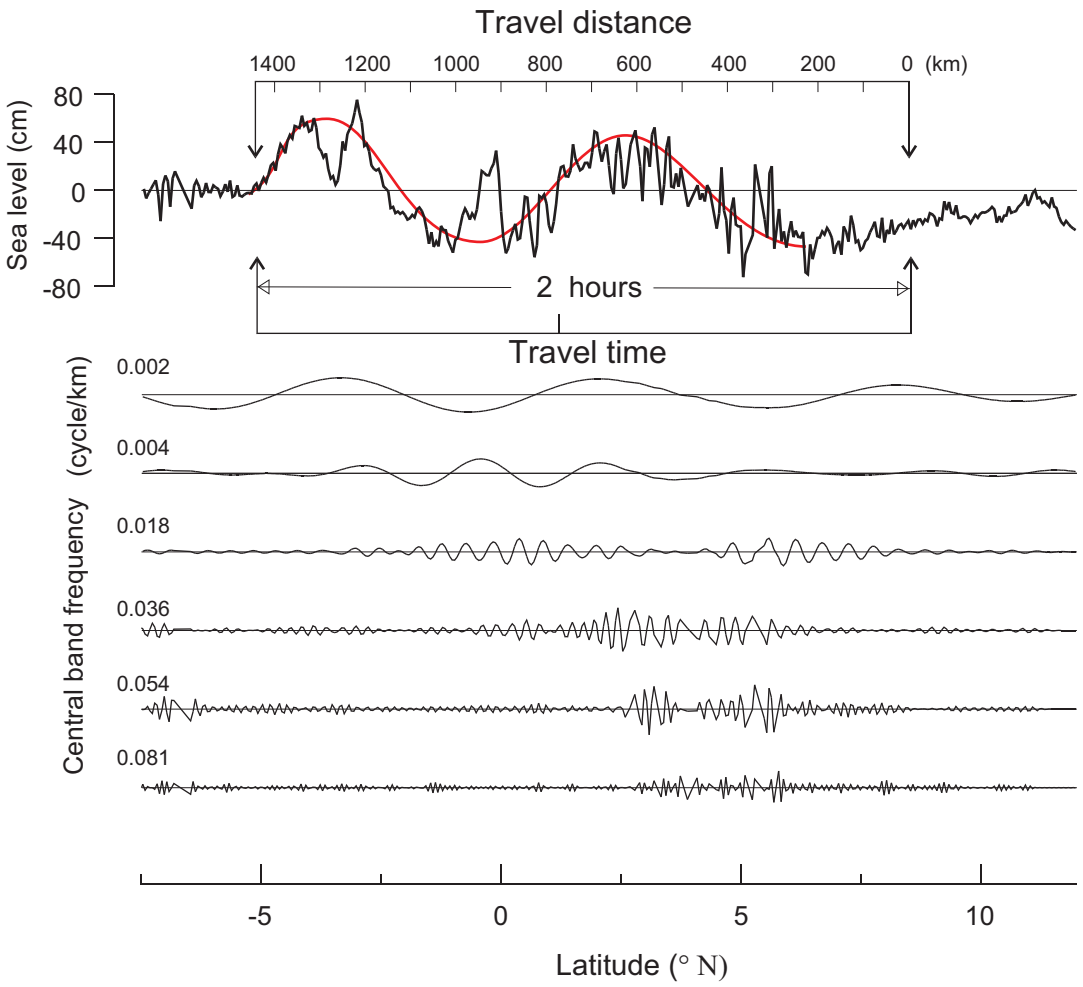
Travel distance
1400
1200
1000
800
600
400
200
0 (km)
Sea level (cm)
80
40
0
-40
-80
2 hours
Travel time
Central band frequency (cycle/km)
0.002
0.004
0.018
0.036
0.054
0.081
-5
0
5
10
Latitude (° N)

Figure 3